Materials Letters 106 (2013) 26–29

Contents lists available at SciVerse ScienceDirect

Materials Letters

journal homepage: www.elsevier.com/locate/matlet

Synthesis, structural and vibrational properties of microcrystalline β-$RbSm(MoO_4)_2$

V.V. Atuchin [a,*], O.D. Chimitova [b], S.V. Adichtchev [c], J.G. Bazarov [b], T.A. Gavrilova [d], M.S. Molokeev [e], N.V. Surovtsev [c], Zh.G. Bazarova [b]

[a] Laboratory of Optical Materials and Structures, Institute of Semiconductor Physics, SB RAS, Novosibirsk 630090, Russia
[b] Laboratory of Oxide Systems, Baikal Institute of Nature Management, SB RAS, Ulan-Ude 670047, Russia
[c] Laboratory of Condensed Matter Spectroscopy, Institute of Automation and Electrometry, SB RAS, Novosibirsk 630090, Russia
[d] Laboratory of Nanodiagnostics and Nanolithography, Institute of Semiconductor Physics, SB RAS, Novosibirsk 630090, Russia
[e] Laboratory of Crystal Physics, Institute of Physics, SB RAS, Krasnoyarsk 660036, Russia

ARTICLE INFO

Article history:
Received 29 January 2013
Accepted 12 April 2013
Available online 1 May 2013

Keywords:
β-$RbSm(MoO_4)_2$
Synthesis
Crystal structure
Raman spectroscopy

ABSTRACT

Low-temperature rubidium samarium dimolybdate, β-$RbSm(MoO_4)_2$, microplates have been prepared by solid state synthesis at 723 K by 70 h and 893 K by 150 h. The crystal structure of β-$RbSm(MoO_4)_2$ has been first refined by the Rietveld method in the space group *Pbcn* with unit cell parameters $a=5.1431(2)$ Å, $b=18.8195(7)$ Å, and $c=8.1641(3)$ Å ($R_B=4.82\%$). The crystal structure of β-$RbSm(MoO_4)_2$ consists of the layers of MoO_4 tetrahedrons corner-sharing with SmO_8 square antiprisms. About 20 narrow Raman lines have been observed in Raman spectra recorded for the β-$RbSm(MoO_4)_2$ powder sample.

© 2013 Elsevier B.V. All rights reserved.

1. Introduction

Molybdate crystals have become of considerable interest because of their interesting structural, luminescent and spectroscopic properties, promising wide applications in optical technologies [1–8]. Among the molybdates reported, the rare-earth containing crystals are of special attention because of their possible application as laser host materials [3,7,9–14]. In many such crystals the rare-earth ions are found in low symmetry positions, which is a key factor for creation of effective ultrafast laser gain media. Searching for new optical materials, it is reasonable to explore the long-discovered but less studied complex molybdate crystals because only fragmentary information can be found and potentials of the crystals are unclear in many aspects [15].

The low-temperature orthorhombic modification β-$RbSm(MoO_4)_2$ is found in the quasi-binary system Rb_2MoO_4–$Sm_2(MoO_4)_3$ at Rb:Sm=1:1, and it exists below $T=1183$–1203 K [16,17]. At $T=1183$–1203 K, β-$RbSm(MoO_4)_2$ transforms to a high-temperature modification α-$RbSm(MoO_4)_2$ of an unknown symmetry. The crystal structure and physical parameters of β-$RbSm(MoO_4)_2$ remains unknown. The present study is aimed at the synthesis and evaluation of microstructural and vibrational parameters of β-$RbSm(MoO_4)_2$. The two-stage solid state synthesis at comparatively low temperatures is selected for β-$RbSm(MoO_4)_2$ preparation to provide precise chemical composition control.

2. Experimental

The powder samples of β-$RbSm(MoO_4)_2$ were prepared using the solid state reaction in platinum crucible. Analytically pure MoO_3 (99.9%), Rb_2CO_3 (99.99%), and Sm_2O_3 (>99.9%) were used as starting materials. To remove the residual water occasionally captured from the air, the Rb_2CO_3 was previously annealed at $T=623$ K. Initially, rubidium and samarium molybdates were prepared. The heat treatment of stoichiometric mixtures was started at $T=723$ K and followed by a step-wise temperature increase up to $T=873$ K (Rb_2MoO_4) and 1073 K ($Sm_2(MoO_4)_3$), respectively. After cooling to room temperature, the Rb_2MoO_4 and $Sm_2(MoO_4)_3$ products were grinded and mixed to obtain the $RbSm(MoO_4)_2$ composition. Then, the powder mixture of the components was preheated at 723 K for ~70 h and then it was fired at 893 K for 150 h to yield the final product. The micromorphology of the powder was observed by SEM with an LEO 1430 device. The measurements, however, were possible only at low accumulation times because of drastic surface charging of the $RbSm(MoO_4)_2$ particles.

The diffraction data for Rietveld analysis were collected over the range of 2θ: 5°–100° at 298 K with a Bruker D8 ADVANCE powder diffractometer in the Bragg–Brentano geometry and linear Vantec detector. The operating parameters were: CuKα radiation, step size

* Corresponding author. Tel.: +7 383 3308889; fax: +7 383 3332771.
E-mail address: atuchin@isp.nsc.ru (V.V. Atuchin).

0167-577X/$ - see front matter © 2013 Elsevier B.V. All rights reserved.
http://dx.doi.org/10.1016/j.matlet.2013.04.039

0.016°, and counting time 1.2 s per step. The X-ray patterns of the title compound were indexed using the ITO program [18]. Almost all reflections were indexed in orthorombic space group *Pbcn* with cell parameters $a=5.145$ Å, $b=18.823$ Å, and $c=8.167$ Å (FOM=45), excepting several minor intensity peaks that could not be assigned definitely. The structure of β-RbSm$(MoO_4)_2$ is isotructural to TlPr$(MoO_4)_2$ [19] and we use the atomic coordinates to refine the structure of β-RbSm$(MoO_4)_2$. All refinements and data processing have been performed by DDM program [20]. The parameters of refinement are reported in Table 1S.

Unpolarized Raman scattering spectra were recorded from the powder sample using a triple grating spectrometer TriVista 777 and a line of $\lambda=532$ nm (200 mW) at room temperature. The spectral resolution during measurements was ~1 cm^{-1} (FWHM). For comparison, a sample of β-RbNd$(MoO_4)_2$ was recorded together with β-RbSm$(MoO_4)_2$. The conditions of β-RbNd$(MoO_4)_2$ preparation can be found elsewhere [10].

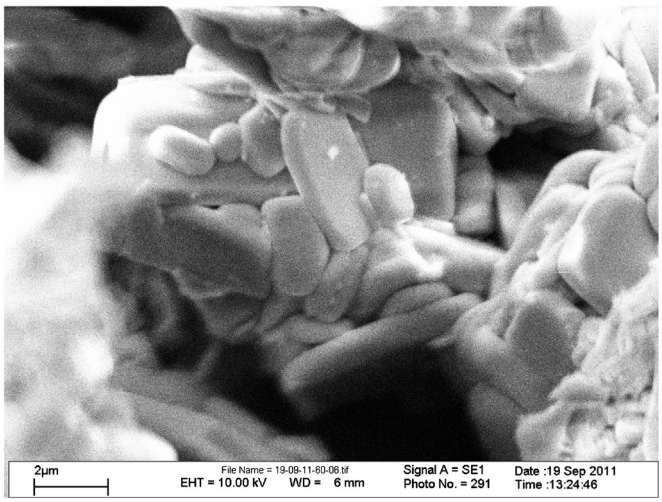

Fig. 1. SEM image of β-RbSm$(MoO_4)_2$ microplates.

3. Results and discussion

The final powder product was of white color with the light orange tint typical of samarium oxides. The micromorphology of β-RbSm$(MoO_4)_2$ particles is shown in Fig. 1. The powder is formed by uniform roundish coalescent grains of ~1–4 μm in diameter. The big facets of the grains are very flat and this indicates the initial stage of equilibrium crystal shape formation. The refinement of the structure in space group *Pbcn* led to a minimal *R*-factor. The coordinates of atoms, isotropic thermal parameters and occupations of atom positions are shown in Table 2S. The experimental (dots) and theoretical (lines) X-ray diffraction patterns of β-RbSm$(MoO_4)_2$ are shown in Fig. 2. Evidently, a good relation between experimental and theoretical curves is achieved. The crystal structure of β-RbSm$(MoO_4)_2$ is shown in Fig. 3 [21]. The structure is formed by complex layers of MoO_4 tetrahedrons shared with SmO_8 square antiprisms by corners. The layers are orthogonal to the *b*-axis of the unit cell and this is a strongly selected crystallographic direction. So, the big flat surfaces of β-RbSm$(MoO_4)_2$ microplates visible in Fig. 1 seem to be orthogonal to the *b* crystallographic axis. Rubidium atoms are located in the gap between MoO_4-SmO_8 layers and are coordinated by six O ions. A set of main interatom bond lengths is presented in Table 3S. In the β-RbSm$(MoO_4)_2$ structure each Mo ion has four Mo–O bonds with comparatively short lengths: L(Mo–O)=1.72–1.85 Å, and two very long Mo–O bonds with as high lengths as L(Mo–O)=2.77–2.79 Å. So, the MoO_6 unit may be considered as a highly distorted octahedron.

Raman spectra of β-RbSm$(MoO_4)_2$ and β-RbNd$(MoO_4)_2$ crystals are shown in Fig. 4. Raman spectra of both crystals are similar and consist of about 20 narrow Raman lines over the spectral range of 30–1000 cm^{-1} (Table 4S). Thus, in the case of β-RbSm$(MoO_4)_2$, in the range of stretched vibrations of MoO_n polyhedra (800–1000 cm^{-1}), the five lines observed have a higher Raman shift. The intensive lines in this spectral range were also found in other complex molybdates [4,7,22–28]. In the stretched Mo–O vibrations range the difference between Raman line positions varies from 0.2% to 0.6% for β-RbSm$(MoO_4)_2$ and β-RbNd$(MoO_4)_2$. Also, the Raman lines of stretched Mo–O vibrations are narrower in β-RbSm$(MoO_4)_2$. Moreover, in the case of RbNd$(MoO_4)_2$. the spectral shape of 943 cm^{-1} (the most intensive stretched Mo–O) line is well

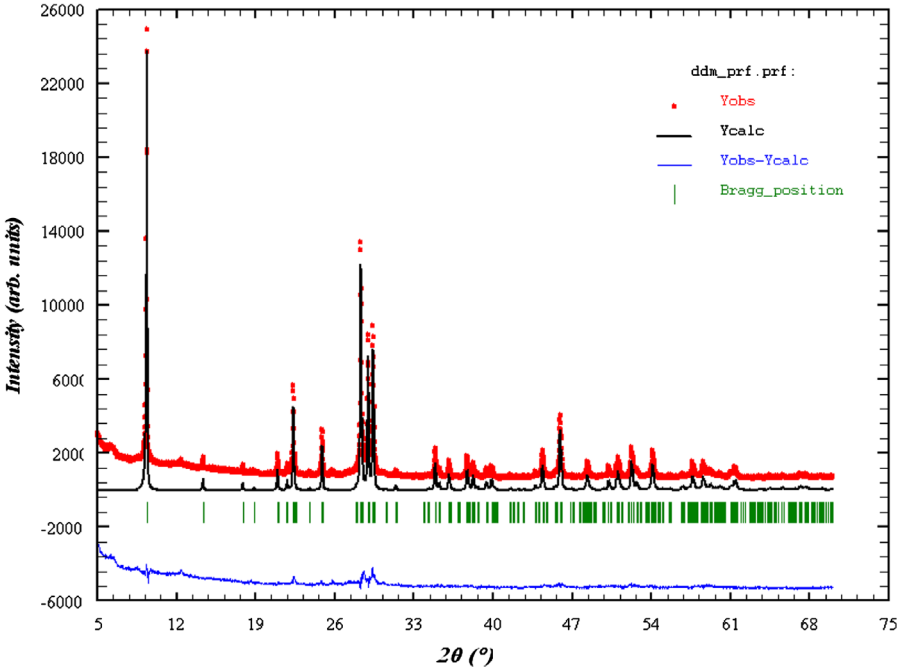

Fig. 2. XRD pattern recorded from the powder sample of β-RbSm$(MoO_4)_2$ at room temperature.

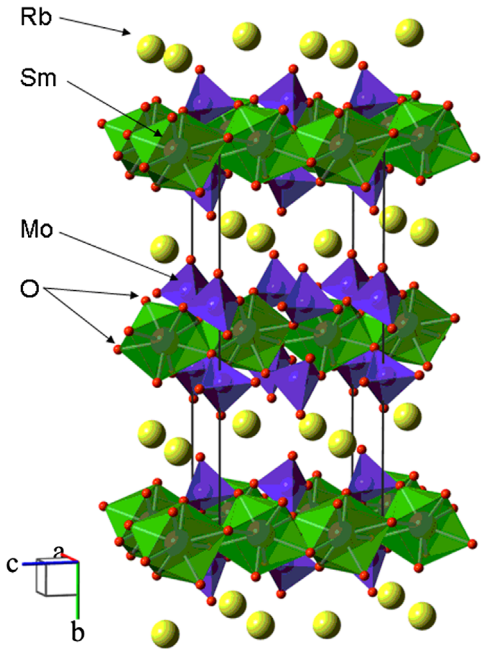

Fig. 3. Crystal structure of β-RbSm$(MoO_4)_2$. Unit cell is outlined. Lone samarium, molybdenum and oxygen atoms are omitted for clarity.

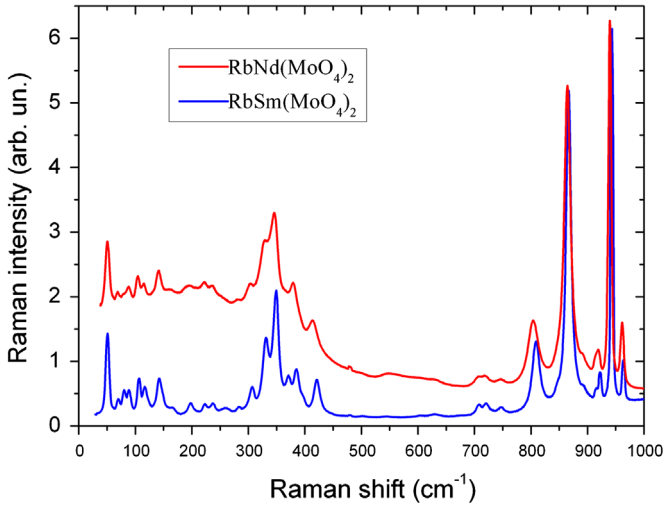

Fig. 4. Raman spectra of β-RbSm$(MoO_4)_2$ and β-RbNd$(MoO_4)_2$.

described by a Voight contour with Gaussin width of 5 cm^{-1} and Lorentzian width of 2 cm^{-1}, while in the case of β-RbSm$(MoO_4)_2$ the spectral shape of 943 cm^{-1} line is rectangular-like with width of 5 cm^{-1}. Thus, the higher vibrational frequency and narrower lines in the case of β-RbSm$(MoO_4)_2$ allow us to conclude that Mo–O vibrations are more harmonic in this crystal in comparison with that of β-RbNd$(MoO_4)_2$). In the low-frequency part of Raman spectrum, the same tendency is observed and the Raman lines recorded from β-RbNd$(MoO_4)_2$) crystal have a lower Raman shift in comparison with that of β-RbSm$(MoO_4)_2$. The observed difference between the counterpart lines is about 0.5–1 cm^{-1}.

4. Conclusions

In the present study, binary molybdate β-RbSm$(MoO_4)_2$ was prepared by solid state synthesis. The plate-like microcrystals of β-RbSm$(MoO_4)_2$ seems to be generated due to anisotropic microcrystal growth. The layered crystal structure refined by the Rietveld method well relates to this supposition. The low symmetry positions are found for Sm^{3+} ions. The spectroscopic parameters of β-RbSm$(MoO_4)_2$ verify the tetrahedral coordination of Mo^{6+} ions and layered character of the crystal lattice. It should be pointed that, according to the phase diagram of the Rb_2MoO_4–$Sm_2(MoO_4)_3$ system, the crystal growth of β-RbSm$(MoO_4)_2$ is possible below $T\sim1200$ K [16,17] to avoid the α↔β phase transition. In this situation, the top seeded solution growth (TSSG) method seems to be optimal.

Acknowledgments

This study is supported by SB RAS under Project 28.12, RFBR (12-02-90806-mol_rf_nr) and the Ministry of Education and Science of the Russian Federation (Contract 16.518.11.7091).

Appendix A. Supporting information

Supplementary data associated with this article can be found in the online version at http://dx.doi.org/10.1016/j.matlet.2013.04.039.

References

[1] Basiev TT, Sobol AA, Voronko YuK, Zverev PG. Spontaneous Raman spectroscopy of tungstate and molybdate crystals for Raman lasers. Opt Mater 2000;15:205–16.
[2] Gao ZL, Tao XT, Yin X, Zhang WG, Jiang MH. Elastic, dielectric, and piezoelectric properties of $BaTeMo_2O_9$ single crystal. Appl Phys Lett 2008;93:252906.
[3] Cai GP, Wang JY, Zhang HJ. Growth and characterization of ferroelectric-ferroelastic $Tb_2(MoO_4)_3$ crystals. Cryst Res Technol 2009;44:1001–4.
[4] Mączka M, Pietraszko A, Paraguassu W, Souza Filho AG, Freire PTC, Mendes Filho J, et al. Structural and vibrational properties of $K_3Fe(MoO_4)_2(Mo_2O_7)$- a novel layered molybdate. J Phys: Condens Matter 2009;21:095402.
[5] Namsaraeva T, Bazarov B, Mikhailova D, Kuratieva N, Sarapulova A, Senyshyn A, et al. Orthomolybdates in the Cs–$Fe^{II,III}$–Mo–O system: $Cs_4Fe(MoO_4)_3$, $Cs_2Fe_2(MoO_4)_3$ and $CsFe_5(MoO_4)_7$. Eur J Inorg Chem 2011:2832–41.
[6] Zhang JJ, Gao ZL, Yin X, Zhang ZH, Sun YX, Tao XT. Investigation of the dielectric, elastic, and piezoelectric properties of $Cs_2TeMo_3O_{12}$ crystals. Appl Phys Lett 2012;101:062901.
[7] Atuchin VV, Grossman VG, Adichtchev SV, Surovtsev NV, Gavrilova TA, Bazarov BG. Structural and vibrational properties of microcrystalline $TlM(MoO_4)_2$ (M=Nd, Pr). Opt Mater 2012;34:812–6.
[8] Lim CS. Cyclic MAM synthesis and upconversion photoluminescence properties of $CaMoO_4$:Er^{3+}/Yb^{3+} particles. Mater Res Bull 2012;47:4220–5.
[9] Tang JF, Chen YJ, Lin YF, Gong XH, Huang JH, Luo ZD, et al. Polarized spectral properties and laser demonstration of Tm^{3+}-doped $LiGd(MoO_4)_2$ crystal. J Opt Soc Am B 2010;27:1769–77.
[10] Atuchin VV, Chimitova OD, Gavrilova TA, Molokeev MS, Kim S-J, Surovtsev NV, et al. Synthesis, structural and vibrational properties of microcrystalline $RbNd(MoO_4)_2$. J Cryst Growth 2011;318:683–6.
[11] Han X, Lahera DE, Serrano MD, Cascales C, Zaldo C. Ultraviolat to infrared refractive indices of tetragonal double tungstate and double molybdate crystals. Appl Phys B 2012;108:509–14.
[12] Li Y, Wang GF, Pan K, Zhou W, Wang C, Fan NY, et al. Control synthesis and luminescence properties of rhombic $NaLn(MoO_4)_2$ submicrocrystals. Cryst Eng Comm 2012;14:5015–20.
[13] Han XM, Calderón-Villajos R, Esteban-Betegón F, Cascales C, Zaldo C. Crystal growth and physical characterization of monoclinic $Li_3Lu_3Ba_2(MoO_4)_2$. A spectrally broadened dosordered crystal for ultrafast mode-locked lasers. Cryst Growth Des 2012;12:3878–87.
[14] Tang JF, Chen YJ, Lin YF, Gong XH, Huang JH, Luo ZD, et al. Tm^{3+}/Ho^{3+} co-doped $LiGd(MoO_4)_2$ crystals as laser gain medium around 2.0 μm. Opt Mater Express 2012;2:1064–75.
[15] Klevtsov PV, Klevtsova RF. Polymorphism of the double molybdates and tungstates of mono- and trivalent metals with composition $M^+R^{3+}(EO_4)_2$. J Struct Chem 1977;18:419–39.
[16] Rybakov VK, Trunov VK. Study of binary molybdates of heavy alkali and rare-earth elements. J Inorg Chem 1971;16:1320–5.
[17] Rybakova TP, Trunov VK. Phase diagrams of rubidium molybdate – lanthanum molybdate and rubidium molybdate – samarium molybdate systems. J Inorg Chem 1973;18:2583–5.
[18] Visser JW. A fully automatic program for finding the unit cell from powder data. J App Crystallogr 1969;2:89–95.

[19] Khobrakova ET, Morozov VA, Belik AA, Lazoryak BI, Khaikina EG, Basovich OM. Structure of some thallium lanthanide double molybdates of composition $TlLn(MoO_4)_2$. Russ J Inorg Chem 2004;49:444–50.
[20] Solovyov LA. Full-profile refienement by derivative difference minimization. J Appl Crystallogr 2004;37:743–9.
[21] Ozawa TC, Kang SJ. Balls&Sticks: easy-to-use structure visualization and animation program. J Appl Cryst 2004;37:679.
[22] Macalik L. Comparison of the spectroscopic and crystallographic data of Tm^{3+} in the different hosts: $KLn(MoO_4)_2$ where Ln=Y,La,Lu and M=Mo,W. J Alloys Compd 2002;341:226–32.
[23] Saraiva GD, Maczka M, Freire PTC, Mendes Filho J, Melo FEA, Hanuza J, et al. Pressure-induced irreversible phase transition in $KSc(MoO_4)_2$. Phys Rev B 2003;67:224108.
[24] Bazarov BG, Sarapulova AE, Klevtsova RF, Glinskaya LA, Fedorov KN, Bazarova ZhG. Synthesis, structure and vibration spectra of the triple molybdates $Tl_5A_{0.5}Hf_{1.5}(MoO_4)_6$, A=Ca,Sr,Ba,Pb. J Alloys Compd 2008;448:325–30.
[25] Atuchin VV, Gavrilova TA, Grigorieva TI, Kuratieva NV, Okotrub KA, Pervukhina NV, et al. Sublimation growth and vibrational microspectrometry of α-MoO_3. J Cryst Growth 2011;318:987–90.
[26] Lim CS. Fabrication and upconversion photoluminescence of CaMoO4:Er^{3+},Yb^{3+} particles by a cyclic microwave-assisted metathetic method. Asian J Chem 2012;24:5659–61.
[27] Maczka M, Souza Filho AG, Paraguassu W, Freire PTC, Mendes Filho J, Hanuza J. Pressure-induced structural phase transitions and amorphization in selected molybdates and tungstates. Prog Mater Sci 2012;57:1335–81.
[28] Godlewska P, Tomaszewicz E, Macalik L, Hanuza J, Ptak M, Tomaszewski PE, et al. Correlation between the structural and spectroscopic parameters for $Cd_{1-3x}Gd_{2x\square x}MoO_4$ solid solutions where □ denotes cationic vacancies. Mater Chem Phys 2013;139:890–6.